A Journal of the Gesellschaft Deutscher Chemiker

Angewandte International Edition

GDCh

Chemie

www.angewandte.org

Accepted Article

Title: Deactivation of Cu-exchanged Automotive Emissions NH3-SCR Catalysts Elucidated with Nanoscale Resolution using Scanning Transmission X-ray Microscopy

Authors: Xinwei Ye, Joel Schmidt, Ru-Pan Wang, Ilse van Ravenhorst, Ramon Oord, Tiehong Chen, Frank de Groot, Florian Meirer, and Bert Marc Weckhuysen

To be cited as: *Angew. Chem. Int. Ed.* 10.1002/anie.201916554
Angew. Chem. 10.1002/ange.201916554

Link to VoR: http://dx.doi.org/10.1002/anie.201916554
http://dx.doi.org/10.1002/ange.201916554

WILEY-VCH

10.1002/anie.201916554

WILEY-VCH

RESEARCH ARTICLE

Deactivation of Cu-exchanged Automotive Emissions NH_3-SCR Catalysts Elucidated with Nanoscale Resolution using Scanning Transmission X-ray Microscopy

Xinwei Ye,[a,b] Joel E. Schmidt,[b] Ru-Pan Wang,[b] Ilse K. van Ravenhorst,[b] Ramon Oord,[b] Tiehong Chen,[a] Frank de Groot,[b] Florian Meirer,[b] Bert M. Weckhuysen*[b]

Abstract: To gain nanoscale insight into the underlying mechanisms of catalyst durability for the selective catalytic reduction (SCR) of NO_X with an ammonia reductant, we employed scanning transmission X-ray microscopy (STXM) to study Cu-exchanged zeolites with the CHA and MFI framework structures before and after a simulated 135,000-mile aging procedure. X-ray absorption near edge structure (XANES) measurements were performed at the Al K- and Cu L-edges using a spot size of 50 × 50 nm^2. The local environment of framework Al, Cu oxidation state and geometric changes were analyzed, showing a multi-factor induced catalytic deactivation. In Cu-exchanged MFI a transformation of Cu^{II} to Cu^{I} and Cu_xO_y was observed as a result of the aging process. We also found a spatial correlation between extra-framework Al and deactivated Cu species near the surface of the zeolite particle. In addition, a weak, positive correlation between Cu^{I} and tri-coordinated Al was present. By inspecting both Al and Cu species within fresh and aged Cu-exchanged zeolites, we conclude that the importance of the preservation of isolated Cu^{II} sites trumps that of Brønsted acid sites for NH_3-SCR activity.

Introduction

Increased fuel efficiency in diesel vehicles results in the undesirable production of environmentally damaging nitrogen oxides (NO_x).[1,2] The commonly employed solution in mobile vehicles is ammonia selective catalytic reduction (NH_3-SCR) of NO_x over Cu-exchanged zeolite catalysts. This was first proposed in a landmark study in 1986 with Cu-exchanged zeolite ZSM-5, which showed high activity, but had insufficient lifetime under the harsh conditions of a real vehicle.[3] To meet the actual requirements of a mobile tailpipe, SCR catalysts must maintain activity throughout a vehicle's lifetime while experiencing a wide range of temperatures between 150 and 550 °C in the presence of steam as well as hydrocarbon and other poisons (e.g. sulfur).[4,5] Another Cu-exchanged zeolite, SSZ-13 (CHA framework), has recently been commercialized for diesel vehicle NH_3-SCR as it provides the required catalytic performance and lifetime. Although it was only first disclosed in the mid-2000s, this material has already been the subject of numerous studies aiming at further improving its performance and lifetime.[5]

To understand the reasons for the high activity and lifetime of Cu-exchanged zeolites in the NH_3-SCR reaction, mechanistic insights about the reaction are needed, which is why the behavior of both the Cu sites and the role of the Brønsted acid sites are topics of extensive investigations.[6] It is commonly agreed upon that the reaction pathway is conducted by the Cu^{II}/Cu^{I} redox cycle under standard NH_3-SCR conditions, where the oxidation of Cu^{I} is considered as the rate-determining step.[7–9] As for Brønsted acid sites, it is proposed that they act as an NH_3 reservoir for Cu sites, but are not involved in forming reactive species.[10] Most of our understanding of Cu speciation and location, and acid properties that might affect the NH_3-SCR reaction, originates from X-ray diffraction (XRD),[11] X-ray absorption spectroscopy (XAS),[8,11–13] ^{27}Al MAS NMR spectroscopy,[12] Fourier-transform infrared spectroscopy (FT-IR),[13] UV-Vis-NIR diffuse reflectance spectroscopy (DRS) [14] and electron paramagnetic resonance spectroscopy (EPR)[15]. These studies of Al and/or Cu properties have led to a more complete picture of sites contributing to NO_x reduction, which gives insight into the catalytic mechanism to guide rational catalyst design. However, to further extend the boundaries of our understanding of NH_3-SCR deactivation, spatially resolved chemical studies at resolutions below 100 nm, that is, significantly smaller than the size of most single catalyst particles, are required, which allow studying the behavior and correlation between species within one catalyst particle in an intuitive way.

So far, only a few techniques could deliver the necessary sub 100 nm spatial resolution and high chemical information content.[16] An atom probe tomography (APT) study of Cu-exchanged zeolites probed the Al and Cu clustering after aging with single atom sensitivity.[17] For the sake of a comprehensive study of local chemical information, Scanning Transmission X-ray Microscopy (STXM) in combination with XANES analysis routinely allows chemical imaging at sub 100 nm spatial resolution, making it a powerful technique to study heterogeneous catalysts in a spatially resolved manner.[18] From a STXM measurement a stack of images is obtained that can be regarded as a three-dimensional data volume. The x axis and y axis make up the field of view (FOV) of the scanned area, while the z axis represents the scanned energy. Therefore, each scanned pixel contains an X-ray absorption spectrum, that is here, more specifically, one XANES spectrum. The power of X-ray chemical imaging lies in the abundant chemical information of detailed local environments revealed in a specific FOV, which enables exploitation of the local relationship between different species.

To reinforce our previous studies on Cu-exchanged zeolites as automotive emissions catalysts,[17,19] here, we report the application of STXM to study the local chemical environment and distribution of Al and Cu in two distinct NH_3-SCR catalysts, namely Cu-SSZ-13 and Cu-ZSM-5. Both fresh and aged

[a] X. Ye, Prof. Dr. T. Chen
School of Materials Science and Engineering
Key Laboratory of Advanced Energy Materials Chemistry (MOE)
Collaborative Innovation Center of Chemical Science and Engineering (Tianjin)
Nankai University
Tianjin 300350, P. R. China
[b] X. Ye, Dr. J. E. Schmidt, R. Wang, I. K. van Ravenhorst, Dr. R. Oord, Prof. Dr. F. de Groot, Dr. F. Meirer, Prof. Dr. ir. B. M. Weckhuysen
Inorganic Chemistry and Catalysis group, Debye Institute for Nanomaterials Science
Utrecht University
Universiteitsweg 99, 3584 CG Utrecht (Netherlands)
Email: b.m.weckhuysen@uu.nl

10.1002/anie.201916554

(135,000-mile simulation[20]) versions of each catalyst material with similar Si/Al ratios and Cu loadings were studied. By comparing the chemical properties of fresh and aged counterparts, the dramatic decrease of NH_3-SCR performance in the most deactivated Cu-exchanged zeolite particles could be attributed to the distortion and aggregation of isolated Cu^{II} expedited by the formation of extra-framework Al species, as revealed by the heterogeneity in the recorded Al and Cu distribution maps. This finding is complemented with conventional characterization methods including XRD, UV-Vis-NIR DRS, FT-IR spectroscopy with NO as probe molecule and ammonia temperature-programmed desorption (NH_3-TPD). The evolution of both Al and Cu species in Cu-exchanged zeolites caused by the aging procedure is discussed and the general properties of the deactivated NH_3-SCR catalysts are pictured in detail. Due to the spatially resolved nature of the STXM data, it was feasible to explore the chemical properties of Al and Cu in different regions within the examined catalyst particle and make statements on the differences between the performances of fresh and aged Cu-SSZ-13 and Cu-ZSM-5.

Results and Discussion

Structure-Performance Relationships

This study was motivated by the NH_3-SCR catalytic performance tested on fresh and aged Cu-exchanged zeolites CHA and MFI. As shown in Figure 1a, for both fresh Cu-exchanged zeolites CHA and MFI, a NO conversion of 80-100 % was achieved over the whole temperature regime, though a slow but steady decrease was observed for Cu-MFI-fresh starting at a temperature of 250 °C and above. Surprisingly, although the aged Cu-CHA underwent a steaming process (simulated aging) before starting the reaction, it exhibited high activity and stability for NO conversion, evidenced by the fact that almost 100 % NO conversion was maintained up to a temperature of 350 °C. In contrast, NO conversion was dramatically reduced for Cu-MFI after the aging process, with the highest observed NO conversion being 60 % at the highest temperature (450 °C). These results are consistent with those reported in numerous studies.[21–23]

By comparing two aged zeolites, Cu-CHA and Cu-MFI, a significant difference in NH_3-SCR activity was observed. One of the most straightforward explanations for this enormous gap in catalytic activity is the differences in stability of the framework structures. However, as indicated by the XRD pattern recorded for our samples, both Cu-CHA and Cu-MFI zeolite samples retained their framework structures after the aging process (Figure S1). On the other hand, it is known that Brønsted acidity originating from framework Al can be hydrolyzed or dehydroxylated upon interacting with steam.[24] Therefore, even though the long-range order of the zeolite structure might be preserved upon steaming, the local structure of framework Al can change. Subsequently, the nature of Cu ions, that relies on the position and density of framework Al, might be affected.

Changes in the local environment of framework Al were evidenced in bulk Al K-edge XANES. It is a relatively straightforward and convincing way to distinguish and quantify Al coordination as compared to high resolution ^{27}Al MAS NMR, a commonly used technique that is, however, sensitive to a diminished signal or line broadening especially when paramagnetic species like Cu^{II} are present.[25,26] The 'bulk single particle XANES' we discuss is the XANES obtained by averaging all XANES recorded for all pixels of a catalyst particle; details can be found in the supporting information. The aging procedure caused a similar effect on Al coordination in both zeolites Cu-CHA and Cu-MFI according to Figure 1b. Although tetrahedral Al, determined by the nature of tetrahedral T sites in the zeolite, was still the dominant species, the emergence of octahedral Al becomes measurable via the occurrence of a shoulder located at the edge position of tetrahedral Al and the peak that becomes visible in the 1569-1575 eV region for both aged zeolites. Furthermore, a pre-edge feature was observed for the aged zeolites, which was more pronounced in the aged Cu-MFI zeolite. This notable low energy feature in the energy range of 1561-1565 eV was assigned to tri-coordinated Al identified by full multiple scattering calculations in a previous study.[26]

A reversible tetrahedral-octahedral transformation of framework Al could be achieved by hydration and dehydration treatment, where either framework Al or Al-OH forms by partial hydrolysis with host water molecules.[27,28] In this way, Al is saturated with H_2O, but without loss of lattice Al. In contrast, intensive steaming undoubtedly accelerates the hydrolysis of the framework Al-O bond, especially at high temperatures, directing

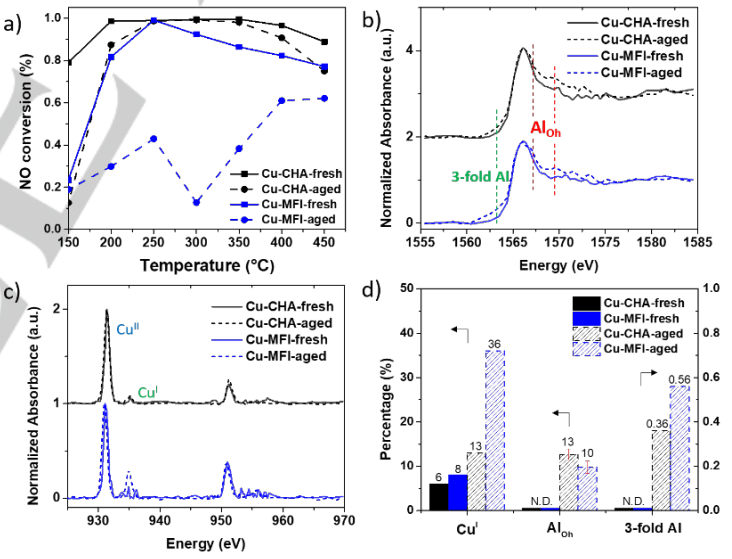

Figure 1. a) NH_3-SCR activity of fresh and aged Cu-exchanged zeolites CHA and MFI. Bulk single particle b) Al K-edge and c) Cu L-edge XANES of fresh and aged Cu-exchanged CHA and MFI. Adsorption features of tetrahedral Al (Al_{Td}), octahedral Al (Al_{Oh}), tri-coordinated Al (3-fold Al), Cu^I and Cu^{II} are indicated. d) Comparison of Cu^I, Al_{Oh} and tri-coordinated Al amount in fresh and aged CHA and MFI. The left axis represents the percentage of Cu^I and Al_{Oh}. The axis on the right indicates the integrated pre-edge area determined from the normalized Al K-edge XANES. Error bars for the percentage of Al_{Oh} were determined from the LSLC fitting. The references information, quantification procedure and results can be found in Figures S2-S4 and Tables S1-S3.

10.1002/anie.201916554

the irreversible formation of extra-framework octahedral Al species.[29] Tri-coordinated Al was proposed to form by dehydroxylation of Brønsted acid sites followed by dealumination in zeolites, but it was mostly deduced indirectly by combining ^{27}Al MAS NMR, EPR and FT-IR spectra recorded after steaming or heating.[30–32] The distorted local environment and large quadrupolar coupling constant of tri-coordinated Al results in the "NMR-invisible" property, so a probe molecule was employed to certify their fine structure.[33,34] The most direct observation of this Al coordination is achieved by XAS via the presence of the aforementioned pre-edge feature that is indicative of the presence of empty mixed s, d, and p orbitals, *i.e.* the nature of unsaturated Al.[26] Previous observations of tri-coordinated Al were reversible in zeolite H-Beta and H-Mordenite, such that it could be restored to tetrahedral Al when exposed to air or wet helium.[26,35] However, in our case, tri-coordinated Al was stable in steamed Cu-exchange CHA and MFI. This irreversible nature implies that the presence of Cu ions could stabilize tri-coordinated Al, which was previously considered as a metastable Al species.

Bulk, single particle Cu L-edge XANES were collected for all samples using the same setup, where the formal oxidation state of copper, indicated by the edge position, is the most straightforward information obtained. A noticeable absorption at ~931.5 eV indicates the predominance of Cu^{II} in all Cu-exchanged zeolite samples (Figure 1c). The effect of steaming on Cu-exchanged CHA was imperceptible. However, in Cu-MFI the aging process induced the reduction of Cu^{II} to Cu^{I}, evidenced by an obvious increase of the Cu^{I} peak. Cu^{I} sites were also observed in FTIR by employing NO as a probe molecule. Apart from the Cu^{I} generated from auto-reduction of $[CuOH]^{+}$, one additional different Cu^{I} site was detected in aged Cu-MFI (Figure S5b). Similar findings of Cu^{I} formation under oxidizing conditions at 400 or 500 °C were previously detected by *in situ* XANES and Rietveld Refinement of *in situ* powder XRD patterns in Cu-SSZ-13.[11,13,36] Additionally, a theoretical study of Cu speciation in CHA indicated that when both H_2O and O_2 exist at temperatures higher than 673 K, Cu^{I} located at a 1Al Cu-exchanged site is thermodynamically favorable.[37] Considering that Cu^{I} has a fully filled d orbital, it is not surprising to observe the formation of Cu^{I}, which then most likely is stabilized by defects generated by the steaming of zeolite Cu-MFI.

Meanwhile, a subtle change of Cu local environment of Cu-MFI after aging is evidenced by a slight shift of the Cu^{II} peak in Figure 1c. The edge position in Cu L-edge XANES is an indicator of Cu^{II} geometric structure due to the crystal field splitting of the d orbital.[38] Although it is difficult to differentiate Cu^{II} coordination geometries in Cu-exchanged zeolites merely by Cu L-edge XANES because of the complexity of the Cu^{II} local environment, the shift of the Cu^{II} edge position can be explained by change of geometric structure or the Cu-O bonding length supported by multiplet calculation (Figures 2, S6), which was also observed in previous studies.[39,40] Therefore, during the steaming process in zeolite Cu-MFI the Cu^{II} geometry plausibly became distorted from the one of a fully saturated Cu^{II} center. In contrast, no change of the Cu^{II} local environment was detected in Cu-CHA, explaining its retained NH_3-SCR activity.

The bulk XANES spectra provide an overview of catalyst properties that correlate with NH_3-SCR performance. Figure 1d summarizes bulk information obtained from bulk single particle

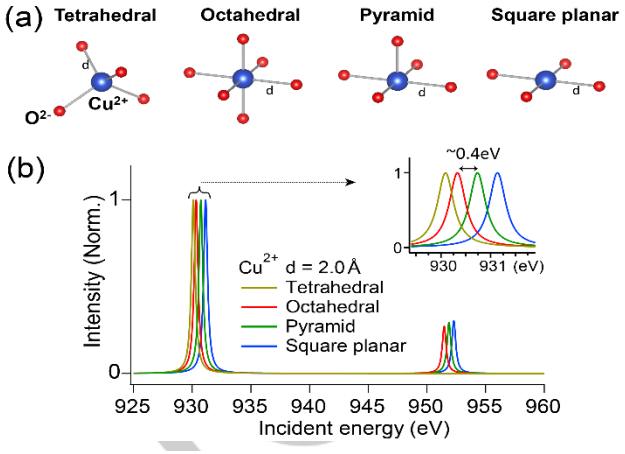

Figure 2. a) Illustration of Cu^{II} in tetrahedral, octahedral, heptahedral (square-pyramidal) and square planar geometries. b) Multiplet calculations of Cu^{II} in different geometric structures with a fixed bond length of 2.0 Å.

XANES of Al and Cu, *i.e.* the relative amounts of Cu^{I}, Al_{Oh} and tri-coordinated Al of fresh/aged Cu-exchanged CHA/MFI. There is a clear difference in the Al coordination between fresh and aged NH_3-SCR active zeolite Cu-CHA indicating that part of the framework tetrahedral Al transformed to octahedral Al and tri-coordinated Al. This dealumination was further evidenced using NH_3-TPD by the loss of Brønsted acid sites after aging (Figure S7), indicating the degree of framework Al degradation was not the dominant factor for catalyst deactivation, especially at temperatures higher than 250 °C as shown in Figure 1a. The limited impact of the Brønsted acidity based on tetrahedral framework Al was previously studied both kinetically and spectroscopically, showing that Brønsted acid sites were not the rate limiting step in the NH_3-SCR reaction cycle and even that extra-framework Al could have a positive influence on the reaction rate.[41–43]

The common feature shared by these three active Cu-exchanged zeolites is the low percentage of Cu^{I}, emphasizing the vital role played by the nature of Cu species in NH_3-SCR. The Cu redox cycle is involved in the NH_3-SCR reaction where both reduction and oxidation half cycles would generate N_2.[7,44,45] In Cu-MFI-aged, a high percentage of Cu sites started their redox cycle from $Cu^{I}(NH_3)_2$ oxidation, which is considered as the rate-limiting step at temperatures lower than 250 °C, and that $Cu^{I}(NH_3)_2$ migrates and then oxidizes to $Cu^{II}(NH_3)_2$.[7,8,46] The local defects generated by steaming might constrain this diffusion of $Cu^{I}(NH_3)_2$, which is linked with the low NO conversion in Cu-MFI-aged. With increasing temperature, the NH_3 ligand releases, and the oxidation of Cu^{I} is thermally accelerated and thus the activity is restored in the higher temperature regions of NH_3-SCR.

In comparison with Cu-MFI, Cu-CHA, with a smaller pore size, was more resistant to hydrothermal treatment with less Al leaching, as previously reported.[21] Therefore, the higher activity and stability of Cu-CHA-aged can be attributed to well-preserved Cu^{II} sites that balance framework Al, in both terms of oxidation state and geometric structure, which enables NH_3 solvation during reaction. In contrast, the Cu^{II} sites in Cu-MFI seemed more susceptible to the aging treatment. Apart from the higher

10.1002/anie.201916554

percentage of Cu^{I} in aged Cu-MFI, our bulk single particle Cu L-edge XANES data together with the multiplet calculations provide evidence for a more distorted local structure of Cu^{II}.

Phase Heterogeneities within Catalyst Particles

The scanned area was processed in a spatially resolved manner by principal component analysis (PCA) and *k*-means clustering after filtering background pixels (more details in supporting information). With this method, the most similar spectra end up in the same cluster, which allows analysis of the spatial distribution of different phases in a sample without using *a priori* knowledge about the phases that are present. Here, it is important to note that the clustering result is only based on spectral correlations and not influenced by any spatial correlations. It should be also added that the number of clusters is assigned manually and not an indication for the actual presence of 3 different spectroscopic phases – *k*-means clustering will always produce the number of clusters used as an input parameter. In this case we intentionally over-clustered the data by using 3 or 4 clusters to check for any spectroscopically distinct, and possibly minor phases, which would emerge in the average XANES of such (over-)clustered data. Therefore, clusters are the result of grouping pixels based on similarity of their spectra.

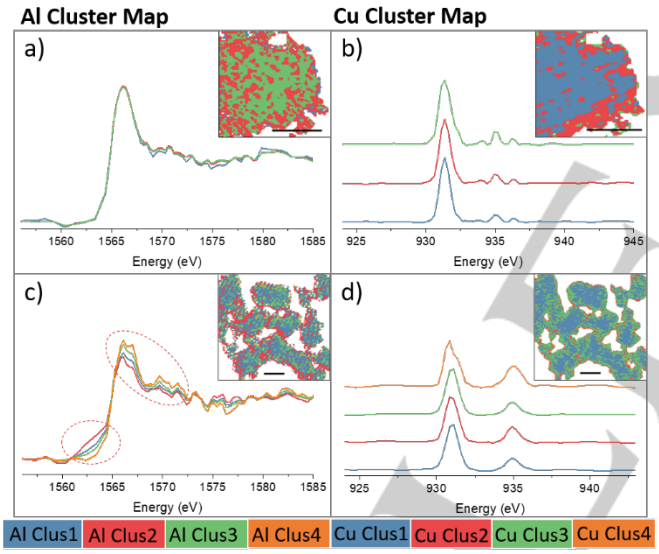

Figure 3 Results of PCA and clustering analysis on the Al and Cu STXM-XANES of Cu-MFI. a) Al K-edge XANES and b) Cu L-edge XANES and the corresponding distribution map (inset) of Cu-MFI-fresh. c) Al K-edge XANES and d) Cu L-edge XANES and the corresponding distribution map (inset) of Cu-MFI-aged. The intensity of the Cu^{II} L-edge was normalized to 1 (as done in the processing of the bulk spectra). In the inserted distribution maps, the scale bars represent 1 µm and the pixel size is 25 × 25 nm^2. The FOV of the inserted map is 2.15 × 2.05 $µm^2$ in a-b), 5.05 × 5.30 $µm^2$ in c-d).

In zeolite Cu-CHA-fresh, a spatially uniform local chemical environment of Al and Cu was found within zeolite particles, indicated by a segmentation result of the measured particles and the corresponding XANES shown in Figure S8. In contrast, in aged Cu-CHA, a slightly lower amount of tri-coordinated Al was observed in Al Clus3, and Cu Clus2, which are preferentially present at the edge of the particle, and showed a slightly significant increase of Cu^{I}. However, the crystal size of zeolite CHA was found to be 100-250 nm by SEM analysis (Figure S9), suggesting that the STXM-measured particle was an agglomerate of nanocrystals. The spatial resolution of 50 nm (beam size) was not high enough to study differences in the chemical distribution of Cu in single nanocrystal zeolite CHA. Thus, the tiny variation among clusters found in Cu-CHA cannot be used as an indicator of Al or Cu heterogeneity at the single crystallite level but only at the nanocrystal agglomerate level.

The crystal size of Cu-exchanged MFI is 0.2 to a few microns, which enables spatial analysis at the single particle level. It is important to emphasize that this zeolite was an industrially manufactured catalyst, making insights especially valuable and difficult to obtain. Figure 3 shows Al and Cu cluster maps of fresh and aged Cu-MFI. Tetrahedral framework Al is distributed homogeneously in fresh Cu-MFI. Although the Cu clusters in Cu-MFI-fresh exhibited a pattern suggesting that Cu Clus1 was surrounded by Cu Clus2, and Cu Clus3 is preferentially located at the edge of the particle, the dissimilarity of the corresponding XANES spectra was found to be negligible within the noise level (Figure 3b); the three clusters were therefore interpreted as identical with respect to Cu oxidation state. Within the noise level we did not find evidence for the presence of more than one spectroscopic phase for both Al and Cu for the single catalyst particle data in fresh Cu-MFI.

As for the deactivated Cu-MFI-aged, statistically significant spatial heterogeneities of spectroscopically different phases of Al and Cu were discriminated within a catalyst particle (Figure 3c, 3d). A pattern of clusters was found, illustrating the slightly different Al geometries of octahedral and three-fold coordination. A strong degree of framework degradation was found to be preferentially located at the external surface of individual zeolite particles, as is evidenced by the distribution of Al Clus2 (representing the phase with tri-coordinated Al), and Al Clus4 (more octahedral Al), in Figure 3c. The oxidation state of Cu within this aged zeolite particle was also not completely uniform. The Cu^{I} percentage was different between clusters and a shoulder peak assigned to Cu^{II} was found in Cu Clus4 (Figure 3d). The Cu^{II} L-edge was split into two contributing peaks with an energy gap of ~1 eV, which could be explained by tetrahedral and square planar Cu^{II} supported by the measured references (Table S1), multiplet calculations and literature,[39] which are diagnosed as hot spots at the edge of the particles (inserted map in Figure 3d). The absolute edge position in Cu L-edge XANES could not give an accurate coordination number without measuring Cu compounds in well-defined geometric structures. However, the observed shoulder with an energy gap of ~1 eV, together with the main peak in the Cu^{II} edge, presents strong evidence for the co-existence of two different geometric structures of square planar and tetrahedral. We have included this discussion to reinforce the importance of carefully considering what can be considered as "real" differences in these analyses.

Spatial Correlation between Al- and Cu-Species

The square planar Cu^{II} in Cu Clus4 (Figure 3d) implied the formation of Cu_xO_y nanoparticles,[47] which are regarded as an inactive species in NH_3-SCR[48]. To more closely investigate their spatial distribution, pixels with an asymmetric Cu^{II} L-edge peak, such as the one shown in Figure 3d, *i.e.* Cu^{II} present in multiple

10.1002/anie.201916554

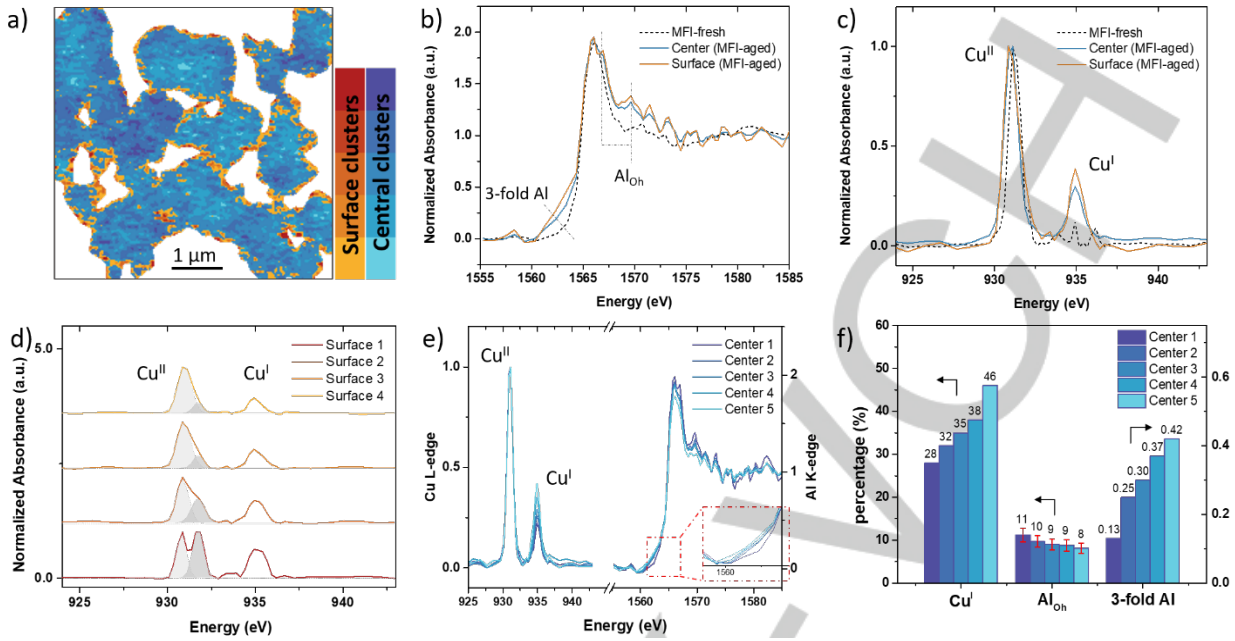

Figure 4. Spatial analysis on individual catalyst particles of aged Cu-exchanged zeolite MFI. a) Cluster map of both surface (orange) and central (blue) area in Cu-MFI-aged, where the color gradient represents a pool of pixels sharing similar spectral features. The classification of pixels was based on the deviation of their Cu L-edge spectra from the average spectrum of all pixels. Surface clusters 1-4 represent region with more degraded Al and Cu species, which were predominantly found on the surface of individual particle. The Central clusters 1-5 mostly describe the bulk information. Sum spectrum of b) Al K-edge XANES and c) Cu L-edge XANES of Surface and Central clusters in comparison with the fresh Cu-MFI. d) Cu L-edge XANES of Surface clusters 1-4 and a deconvolution of the Cu^{II} peak. e) Cu L-edge XANES and Al K-edge XANES of Central clusters 1-5. f) The relative amounts of Cu^{I}, Al$_{Oh}$ and tri-coordinated Al determined based on the spectra in e). The left axis represents percentage, whereas the right axis represents the integrated area of the pre-edge region in Al K-edge XANES.

geometric structures, were selected and divided into four groups that varied in their fraction of square planar Cu^{II}. It is clear from Figure 4a that these pixels with square planar Cu^{II} were almost exclusively located at the surface of the individual particles, that is, within a few hundred nanometers of the surface of each catalyst particle. This distribution implies that the aggregation of Cu happened near the particle surface, where it then gradually formed Cu_xO_y nanoparticles. This partial Cu^{II} agglomeration in Cu-MFI-aged was also evidenced in UV-Vis-NIR DRS spectra (Figure S10), showing the additional absorption of Cu_xO_y at around 40,000 cm^{-1} when compared to its fresh counterpart.[14] These results strongly indicate that part of Cu^{II} in Cu-MFI was no longer present as isolated sites after aging.

The deactivation of the Cu-exchanged MFI has previously been linked to the affinity of Cu to form Cu-Cu and Cu-Al bonds, indicating the formation of Cu_xO_y nanoparticles or a $CuAl_xO_y$ spinel phase, respectively.[12,17,49] By correlating the Al and Cu STXM data we could obtain additional information about the spatial correlation between Al and Cu: the very surface area containing a large fraction of Cu_xO_y and Cu^{I} also shows partial destruction of the zeolite framework (Figures 4b, 4c, S11). Due to the co-occurrence of octahedral Al and tetrahedral Cu, a $CuAl_xO_y$ spinel phase cannot be excluded in our case. The destroyed surface layer of Cu-MFI-aged can be explained by the fact that the surface area of each zeolite particle was the first region that is exposed to steam, and therefore experienced the most severe steaming treatment. The detachment of extra-framework Al then induces migration and subsequently aggregation of Cu ions because it is no longer necessary to have a cation to balance the negative charge from framework Al. In turn, the aggregation of freed, isolated Cu ions causes them to lose their charge balance ability, which further enhances the severe framework damage in zeolite MFI. The interplay between degraded Al and Cu eventually leads to the zoning of inactive species that might further limit diffusion of reactants and products through the catalyst particle because of the collapse and blockage of zeolite channels on the catalyst particle surface. All of this leads to the “perfect storm” for deactivation.

Severe degradation of Al and Cu species was predominately found in the region of around 250 nm from the surface. However, the other areas within particles that were less degraded reveal the more general chemical properties of the catalyst. Hence, for a more detailed analysis of these areas, pixels with square planer Cu^{II} composite, *i.e.* the surface region marked in orange in Figure 4a, were filtered before inspecting the main body of each particle of Cu-MFI-aged. Thus, Cu L-edge XANES of the remaining pixels showed a single Cu^{II} L-edge peak representing distorted tetrahedral Cu^{II} or octahedral Cu^{II}. The classification of the central part of catalyst particle was achieved by examining the first two Principal Components (PC) based on the fact that PC1 closely resembles the average spectrum of all pixels (after background removal) and PC2 represents the strongest deviation from PC1 (being an orthonormal basis vector to PC1 and capturing the second largest variance in the data). It

is clear in Figure S12 that the pixels with a higher contribution of PC2 contained a lower percentage of Cu^{I}. The clusters Center 1-5 were labeled such that the Cu^{I} amount increased when going from cluster Center 1 to Center 5. The corresponding Al K-edge XANES and Cu L-edge XANES of each cluster are shown in Figure 4e.

The clusters Center 1-5 in Figure 4e exhibit a spatially random pattern, suggesting that the transformation of Cu^{II} to Cu^{I} does not have a preferred location or direction within individual zeolite particles. Based on the estimated amount of degraded Al species obtained from LSLC fitting, all these clusters have a comparable percentage of octahedral Al but vary in tri-coordinated Al, as illustrated in the zoom-in to the pre-edge region in Figure 4e. The trend of increasing three-fold Al coordination when going from cluster Center 1 to Center 5 was accompanied by an increasing Cu^{I} percentage. Undoubtedly, hydrolyzation or hydroxylation of Brønsted acidity would destroy the framework structure, directing the formation of defect sites consisting of tri-coordinated Al, such as Al-OH and AlO^{+}.[26] Subsequently AlOOH, $Al(OH)_2^{+}$ and $Al(OH)_3$ might be formed in the presence of water.[12,50] On the other hand, Cu^{I} was created by auto-reduction of either $[CuOH]^{+}$ or Cu^{II}. The reduction of Cu^{II} was proposed to associate with a thermally-driven decomposition of H_2O at temperatures higher than 300 °C, accompanied by the formation of a proton that can balance the framework charge.[51] However, independent of how Cu^{I} is generated, Cu^{I} could be stabilized by tri-coordinated Al if it is adjacent to the degraded Al site. Finally, considering the intimate interaction between leached Al and Cu, the formation of $CuAl_xO_y$ phase cannot be excluded,[12] which was also proposed from APT studies[17,19] and XAS studies[23].

We have elucidated the deactivation of Cu-exchanged zeolites in terms of local environment and the spatial distribution of both Al and Cu. The sensitivity of XAS to the geometric structure enabled us to discover the “NMR invisible” tri-coordinated Al, which exists in both aged Cu-CHA and aged Cu-MFI. Since dealumination was found in NH_3-SCR active catalyst Cu-CHA-aged, the limited degree of framework destruction was not the main reason for the loss of activity. Instead, the loss of isolated Cu sites, which transformed into Cu_xO_y nanoparticles or a $CuAl_xO_y$ spinal phase and was largely located on the particle surface, is more detrimental to the reaction. It was previously inferred from XPS and calorimetry upon adsorption of the probe molecule NH_3 that the location of defect sites in zeolite ZSM-5 is mainly concentrated on the external surface of the zeolite crystals.[52] Via our spatial analysis of the data recorded for zeolite Cu-MFI-aged we could now directly visualize this, revealing that the most degraded framework structure is located at the edges of the individual catalyst particles and goes along with the formation of inactive Cu_xO_y nanoparticles, which further limit the accessibility of less destroyed Cu sites in the central part of catalyst particles due to framework collapse and channel blockage near surface. This observed Al and Cu zoning is a good example of nanoscale destruction in industrial catalysts, which is caused by surface migration of nanoparticles.[53] The discovery of this minority species of Cu_xO_y at the surface (4555 surface pixels from a total of 29759 analyzed pixels) illustrates the power of STXM for nanoscale spatial analysis of catalyst particles.

Conclusion

The observed variations in catalytic activity and stability between fresh and aged Cu-exchanged zeolites with different framework structures (CHA and MFI) motivated a detailed study of the deactivation factors with respect to zeolite framework structure, Al species, and Cu species. Therefore, we employed STXM, which combines the main functions of X-ray absorption spectroscopy (XAS) and high-resolution imaging, providing abundant information about the local chemical environment in the form of a chemical map of fresh and aged Cu-exchanged zeolites. Our results indicate that although the degradation of tetrahedral framework Al to octahedral Al or tri-coordinated Al caused the loss of Brønsted acid sites, NH_3-SCR activity was maintained in Cu-exchanged CHA even after aging, which is attributed to the hydrothermally stable framework structure and well-preserved Cu^{II}. For Cu-exchanged MFI, the deactivation of NH_3-SCR was induced by the evolution of isolated Cu^{II} to both Cu^{I} and Cu_xO_y, resulting in a scarcity of isolated Cu^{II} in aged Cu-MFI. The spatial distribution of both Al and Cu species was explored by inspecting single-pixel spectra, revealing spatial correlations between species and information that is lost in bulk data. We observed zoning of extra-framework Al, Cu^{I} and Cu_xO_y on the surface of every individual catalyst particle of the most deactivated zeolite, Cu-MFI-aged. Then, by investigating the main body of each catalyst particle, *i.e.* excluding the degraded surface regions, a plausible spatial correlation between tri-coordinated Al and Cu^{I} was established. Overall, we can conclude that the loss of isolated Cu sites is detrimental to NH_3-SCR performance. Considering the interdependence between framework Al and isolated Cu species, further investigations of a more durable NH_3-SCR catalyst should emphasize the stabilization of isolated Cu active sites. In case of Cu-exchanged zeolites, preservation of isolated Cu relies on the stability of an Al-containing framework, that is a hydrothermally stable of zeolite lattice, as a critical factor for NH_3-SCR.

Acknowledgements

This work is supported by the Netherlands Organization for Scientific Research (NWO) in the frame of a Gravitation Program (MCEC, Multiscale Catalytic Energy Conversion). X.Y. acknowledges support from China Scholarship Council (CSC). This research used resources of the Advanced Light Source (ALS), which is a U.S. DOE Office of Science User Facility under contract no. DE-AC02-05CH11231. J.E.S. has received funding from the European Union’s Horizon 2020 research and innovation program under the Marie Sklodowska-Curie grant agreement No. 702149.

Keywords: Zeolite • Automotive Catalysis • Copper • X-ray Microscopy • Catalyst Deactivation

[1] P. Granger, V. I. Parvulescu, *Chem. Rev.* **2011**, *111*, 3155–3207.

[2] S. Brandenberger, O. Kröcher, A. Tissler, R. Althoff, *Catal. Rev.* **2008**, *50*, 492–531.

[3] M. Iwamoto, H. Furukawa, Y. Mine, F. Uemura, S. Mikuriya, S.

Kagawa, *J. Chem. Soc. Chem. Commun.* **1986**, 1272-1273.

[4] J. H. Kwak, R. G. Tonkyn, D. H. Kim, J. Szanyi, C. H. F. Peden, *J. Catal.* **2010**, *275*, 187–190.

[5] A. M. Beale, F. Gao, I. Lezcano-Gonzalez, C. H. F. Peden, J. Szanyi, *Chem. Soc. Rev.* **2015**, *44*, 7371–7405.

[6] U. Deka, I. Lezcano-Gonzalez, B. M. Weckhuysen, A. M. Beale, *ACS Catal.* **2013**, *3*, 413–427.

[7] C. Paolucci, I. Khurana, A. A. Parekh, S. Li, A. J. Shih, H. Li, J. R. Di Iorio, J. D. Albarracin-Caballero, A. Yezerets, J. T. Miller, W. N. Delgass, F. H. Ribeiro, W. F. Schneider, R. Gounder, *Science* **2017**, *357*, 898–903.

[8] A. Marberger, A. W. Petrov, P. Steiger, M. Elsener, O. Kröcher, M. Nachtegaal, D. Ferri, *Nat. Catal.* **2018**, *1*, 221–227.

[9] K. A. Lomachenko, E. Borfecchia, C. Negri, G. Berlier, C. Lamberti, P. Beato, H. Falsig, S. Bordiga, *J. Am. Chem. Soc.* **2016**, *138*, 12025–12028.

[10] F. Gao, N. M. Washton, Y. Wang, M. Kollár, J. Szanyi, C. H. F. Peden, *J. Catal.* **2015**, *331*, 25–38.

[11] C. W. Andersen, E. Borfecchia, M. Bremholm, M. R. V. Jørgensen, P. N. R. Vennestrøm, C. Lamberti, L. F. Lundegaard, B. B. Iversen, *Angew. Chem. Int. Ed.* **2017**, *56*, 10367–10372.

[12] P. N. R. Vennestrøm, T. V. W. Janssens, A. Kustov, M. Grill, A. Puig-Molina, L. F. Lundegaard, R. R. Tiruvalam, P. Concepción, A. Corma, *J. Catal.* **2014**, *309*, 477–490.

[13] F. Giordanino, E. Borfecchia, K. A. Lomachenko, A. Lazzarini, G. Agostini, E. Gallo, A. V. Soldatov, P. Beato, S. Bordiga, C. Lamberti, *J. Phys. Chem. Lett.* **2014**, *5*, 1552–1559.

[14] R. Oord, I. C. ten Have, J. M. Arends, F. C. Hendriks, J. Schmidt, I. Lezcano-Gonzalez, B. M. Weckhuysen, *Catal. Sci. Technol.* **2017**, *7*, 3851–3862.

[15] A. Godiksen, F. N. Stappen, P. N. R. Vennestrøm, F. Giordanino, S. B. Rasmussen, L. F. Lundegaard, S. Mossin, *J. Phys. Chem. C* **2014**, *118*, 23126–23138.

[16] I. L. C. Buurmans, B. M. Weckhuysen, *Nat. Chem.* **2012**, *4*, 873–886.

[17] J. E. Schmidt, R. Oord, W. Guo, J. D. Poplawsky, B. M. Weckhuysen, *Nat. Commun.* **2017**, *8*, 1666.

[18] F. Meirer, B. M. Weckhuysen, *Nat. Rev. Mater.* **2018**, *3*, 324–340.

[19] J. E. Schmidt, X. Ye, I. K. van Ravenhorst, R. Oord, D. A. Shapiro, Y. Yu, S. R. Bare, F. Meirer, J. D. Poplawsky, B. M. Weckhuysen, *ChemCatChem* **2019**, *11*, 488–494.

[20] S. J. Schmieg, S. H. Oh, C. H. Kim, D. B. Brown, J. H. Lee, C. H. F. Peden, D. H. Kim, *Catal. Today* **2012**, *184*, 252–261.

[21] D. W. Fickel, E. D'Addio, J. A. Lauterbach, R. F. Lobo, *Appl. Catal. B Environ.* **2011**, *102*, 441–448.

[22] J. H. Kwak, D. Tran, S. D. Burton, J. Szanyi, J. H. Lee, C. H. F. Peden, *J. Catal.* **2012**, *287*, 203–209.

[23] P. N. R. Vennestrøm, T. V. W. Janssens, A. Kustov, M. Grill, A. Puig-Molina, L. F. Lundegaard, R. R. Tiruvalam, P. Concepción, A. Corma, *J. Catal.* **2014**, *309*, 477–490.

[24] S. Malola, S. Svelle, F. L. Bleken, O. Swang, *Angew. Chem. Int. Ed.* **2012**, *51*, 652–655.

[25] A. M. Beale, A. M. J. van der Eerden, D. Grandjean, A. V Petukhov, A. D. Smith, B. M. Weckhuysen, *Chem. Commun.* **2006**, 4410-4412.

[26] J. A. Van Bokhoven, A. M. J. Van der Eerden, D. C. Koningsberger, *J. Am. Chem. Soc.* **2003**, *125*, 7435–7442.

[27] B. H. Wouters, T. H. Chen, P. J. Grobet, *J. Am. Chem. Soc.* **1998**, *120*, 11419–11425.

[28] I. J. Drake, Y. Zhang, M. K. Gilles, C. N. Teris Liu, P. Nachimuthu, R. C. C. Perera, H. Wakita, A. T. Bell, *J. Phys. Chem. B* **2006**, *110*, 11665–11676.

[29] J. A. Van Bokhoven, D. C. Koningsberger, P. Kunkeler, H. van Bekkum, *J. Catal.* **2002**, *211*, 540–547.

[30] F. Deng, Y. Du, C.-H. Ye, *Magn. Reson. Imaging* **1996**, *14*, 945–946.

[31] J. Brus, L. Kobera, W. Schoefberger, M. Urbanová, P. Klein, P. Sazama, E. Tabor, S. Sklenak, A. V. Fishchuk, J. Dědeček, *Angew. Chem. Int. Ed.* **2015**, *54*, 541–545.

[32] R. M. Mihályi, M. Kollár, P. Király, Z. Karoly, V. Mavrodinova, *Appl. Catal. A Gen.* **2012**, *417–418*, 76–86.

[33] X. Yi, K. Liu, W. Chen, J. Li, S. Xu, C. Li, Y. Xiao, H. Liu, X. Guo, S.-B. Liu, A. Zheng, *J. Am. Chem. Soc.* **2018**, *140*, 10764–10774.

[34] S. Xin, Q. Wang, J. Xu, Y. Chu, P. Wang, N. Feng, G. Qi, J. Trébosc, O. Lafon, W. Fan, F. Deng, *Chem. Sci.* **2019**, *10*, 10159–10169.

[35] L. A. Bugaev, J. A. Van Bokhoven, A. P. Sokolenko, Y. V. Latokha, L. A. Avakyan, *J. Phys. Chem. B* **2005**, *109*, 10771–10778.

[36] E. Borfecchia, K. A. Lomachenko, F. Giordanino, H. Falsig, P. Beato, A. V. Soldatov, S. Bordiga, C. Lamberti, *Chem. Sci.* **2015**, *6*, 548–563.

[37] C. Paolucci, A. A. Parekh, I. Khurana, J. R. Di Iorio, H. Li, J. D. Albarracin Caballero, A. J. Shih, T. Anggara, W. N. Delgass, J. T. Miller, F. H. Ribeiro, R. Gounder, W. F. Schneider, *J. Am. Chem. Soc.* **2016**, *138*, 6028–6048.

[38] S. J. George, S. P. Cramer, M. D. Lowery, E. I. Solomon, *J. Am. Chem. Soc.* **1993**, *115*, 2968–2969.

[39] K. Shimizu, H. Maeshima, H. Yoshida, A. Satsuma, T. Hattori, *Phys. Chem. Chem. Phys.* **2001**, *3*, 862–866.

[40] M. Grioni, J. B. Goedkoop, R. Schoorl, F. M. F. de Groot, J. C. Fuggle, F. Schäfers, E. E. Koch, G. Rossi, J.-M. Esteva, R. C. Karnatak, *Phys. Rev. B* **1989**, *39*, 1541–1545.

[41] S. A. Bates, A. A. Verma, C. Paolucci, A. A. Parekh, T. Anggara, A. Yezerets, W. F. Schneider, J. T. Miller, W. N. Delgass, F. H. Ribeiro, *J. Catal.* **2014**, *312*, 87–97.

[42] I. Lezcano-Gonzalez, U. Deka, B. Arstad, A. Van Yperen-De Deyne, K. Hemelsoet, M. Waroquier, V. Van Speybroeck, B. M. Weckhuysen, A. M. Beale, *Phys. Chem. Chem. Phys.* **2014**, *16*, 1639–1650.

[43] T. V. W. Janssens, H. Falsig, L. F. Lundegaard, P. N. R. Vennestrøm, S. B. Rasmussen, P. G. Moses, F. Giordanino, E. Borfecchia, K. A. Lomachenko, C. Lamberti, S. Bordiga, A. Godiksen, S. Mossin, P. Beato, *ACS Catal.* **2015**, *5*, 2832–2845.

[44] M. Moreno-González, R. Millán, P. Concepción, T. Blasco, M. Boronat, *ACS Catal.* **2019**, *9*, 2725-2738.

[45] C. Paolucci, A. A. Verma, S. A. Bates, V. F. Kispersky, J. T. Miller, R. Gounder, W. N. Delgass, F. H. Ribeiro, W. F. Schneider, *Angew. Chem. Int. Ed.* **2014**, *53*, 11828–11833.

[46] F. Gao, D. Mei, Y. Wang, J. Szanyi, C. H. F. Peden, *J. Am. Chem. Soc.* **2017**, *139*, 4935–4942.

[47] J. B. Forsyth, S. Hull, *J. Phys. Condens. Matter* **1991**, *3*, 5257–

10.1002/anie.201916554

5261.

[48] A. Wang, Y. Chen, E. D. Walter, N. M. Washton, D. Mei, T. Varga, Y. Wang, J. Szanyi, Y. Wang, C. H. F. Peden, F. Gao, *Nat. Commun.* **2019**, *10*, 1137.

[49] J. Song, Y. Wang, E. D. Walter, N. M. Washton, D. Mei, L. Kovarik, M. H. Engelhard, S. Prodinger, Y. Wang, C. H. F. Peden, F. Gao, *ACS Catal.* **2017**, *7*, 8214–8227.

[50] P. A. Jacobs, H. K. Beyer, *J. Phys. Chem.* **1979**, *83*, 1174–1177.

[51] P. H. Kasai, R. J. Bishop, *J. Phys. Chem.* **1977**, *81*, 1527–1529.

[52] V. Bolis, S. Maggiorini, L. Meda, F. D'Acapito, G. T. Palomino, S. Bordiga, C. Lamberti, *J. Chem. Phys.* **2000**, *113*, 9248–9261.

[53] J. A. Moulijn, A. E. van Diepen, F. Kapteijn, *Appl. Catal. A Gen.* **2001**, *212*, 3–16.

10.1002/anie.201916554

WILEY-VCH

RESEARCH ARTICLE

The deactivation of NO_x reduction catalysts based on Cu-exchanged SSZ-13 and ZSM-5 zeolites was studied by Scanning Transmission X-ray Microscopy (STXM), which enables a spatial analysis of the local environment of both Al and Cu species at nanoscale resolution. The importance of isolated Cu species was proven and a correlation between zeolite lattice destruction and an inactive Cu phase was established.

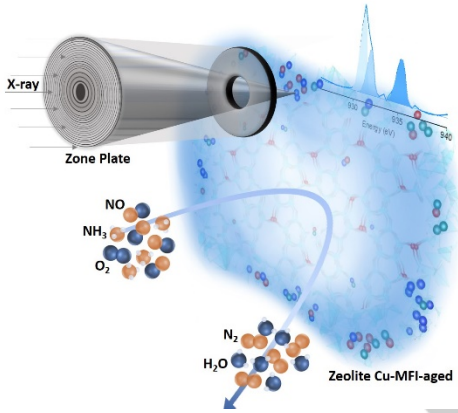

*Xinwei Ye, Joel E. Schmidt, Ru-Pan Wang, Ilse K. van Ravenhorst, Ramon Oord, Tiehong Chen, Frank de Groot, Florian Meirer, Bert M. Weckhuysen**

Page No. – Page No.

Deactivation of Cu-exchanged Automotive Emissions NH_3-SCR Catalysts Elucidated with Nanoscale Resolution using Scanning Transmission X-ray Microscopy